This is the peer-reviewed, final accepted version for American Mineralogist, published by the Mineralogical Society of America.
The published version is subject to change. Cite as Authors (Year) Title. American Mineralogist, in press.
DOI: https://doi.org/10.2138/am-2022-8055. http://www.minsocam.org/

Manuscript AM 8055R - Revision 1

Fission-track etching in apatite: A model and some implications

RAYMOND JONCKHEERE[1,*], CAROLIN ASLANIAN[1], BASTIAN WAUSCHKUHN[1], AND LOTHAR RATSCHBACHER[1]

[1]Geologie, TU Bergakademie Freiberg, 09599 Freiberg, Germany

ABSTRACT

From their formation, fission tracks are complex structures, onto which their thermal histories come to be imprinted. Track etching leaves elongated voids whose lengths and orientations are used for reconstructing these histories. It is thus important to understand etching for interpreting track data. We revive an existing dissolution model which explains the geometries and dimensions of etched fission tracks in apatite. It implies that on continued etching the track contours come to reflect the minimum and maximum apatite etch rates, at the same time that all trace of the track structure is erased. We cannot derive valid etch rates from the dimensions of the track openings or from the length increase of step-etched confined tracks. The roundedness of the track tips is not a measure of etching progress. Understanding the contours of confined tracks does permit in most cases to calculate their true etch times. We propose to exploit this fact to set an etch-time window, and to model the confined-track data in this interval. The excluded measurements will be those of the least-etched and most-etched tracks. This numerical loss is offset by the fact that an etch-time window relaxes the requirement of a fixed immersion time, and a longer immersion multiplies the measurable confined tracks. This calls for no changes to existing procedures if the etch-time windows for different protocols give consistent results. The length data for apatites with different compositions could become comparable if their etch-time windows were linked to a compositional parameter.

Keywords: Apatite, fission track, etching, effective etch time, surface track, confined track

*Email: Raymond.Jonckheere@geo.tu-freiberg.de

Always consult and cite the final, published document. See http:/www.minsocam.org or GeoscienceWorld

This is the peer-reviewed, final accepted version for American Mineralogist, published by the Mineralogical Society of America.
The published version is subject to change. Cite as Authors (Year) Title. American Mineralogist, in press.
DOI: https://doi.org/10.2138/am-2022-8055. http://www.minsocam.org/

INTRODUCTION

Fission tracks in apatite are ~20 μm long (Bhandari et al. 1971; Jonckheere 2003) and ~10 nm wide (Paul and Fitzgerald 1992; Paul 1993; Li et al. 2011; 2012; 2014), too thin to observe with a microscope. Polished grain mounts are therefore etched for fission-track dating and thermal history modelling. Etching creates micrometer-wide channels along the track axes, which can be counted and measured with an optical microscope. The average etchable length of a fission track in apatite is ~16 μm or less, depending on the temperatures that it has experienced, but also on its orientation, the apatite composition and the etching protocol (Tamer et al. 2019). The effects of temperature, orientation and composition have been studied and integrated in quantitative models. These studies have become too numerous to list but Tables 5 and 6 of Wauschkuhn et al. (2015) give an overview.

Investigations of apatite (Fleischer and Price 1964; Patel et al. 1967), zircon (Krishnaswami et al. 1974; Gleadow and Lovering 1977) and titanite (Naeser 1967; Gleadow 1978) showed that track revelation is anisotropic and that the crystallographic orientations of the etched surfaces influence their etching characteristics and the appearance of the etched tracks. Later studies investigated the influence of etching on the track densities, e.g., for apatite: Green and Durrani (1978), Poupeau et al. (1980), Watt and Durrani (1985), Singh et al. (1986), Sandhu et al. (1988a, b), and Jafri et al. (1990). Interest waned after the ζ-calibration was adopted (Hurford 1990a, b), which obviated explicit counting efficiencies. Its intended application to single-grain dating implies that the tracks should be counted in slow-etching faces with high etching efficiencies, e.g., the prism faces of apatite (Gleadow 1981). This is a lasting result of the investigations of anisotropic fission-track etching. Beginning before, but for the most part after the ζ-watershed, etching experiments were aimed at defining suitable protocols for etching confined fission tracks in advance of comprehensive annealing experiments, e.g., Laslett et al. (1984), Green et al. (1986), Crowley et al. (1991), Carlson et al. (1999), Barbarand et al. (2003), Ravenhurst et al. (2003), and Tello et al. (2006). Other studies addressed certain fundamental aspects of fission-track etching in apatite (Hejl 1995; Jonckheere and Van den haute 1996; Jonckheere et al. 2005; 2007; 2017; 2019; Murrell et al. 2009; Moreira et al. 2010; Sobel and Seward 2010; Tamer et al. 2019; Tamer and Ketcham 2020; Aslanian et al. 2021).

Several models have been proposed to account for the appearance of etched tracks in isotropic and anisotropic detectors. All are based on the premise that the track geometries result from dissolution

Always consult and cite the final, published document. See http:/www.minsocam.org or GeoscienceWorld

This is the peer-reviewed, final accepted version for American Mineralogist, published by the Mineralogical Society of America.
The published version is subject to change. Cite as Authors (Year) Title. American Mineralogist, in press.
DOI: https://doi.org/10.2138/am-2022-8055. http://www.minsocam.org/

of the damaged core at a rate v_T (track etch rate) along the track axis and of the undamaged detector at a rate v_B (bulk etch rate) in all other directions. Etched-track profiles were calculated for isotropic v_B and constant and variable v_T (Fleischer et al. 1969; Henke and Benton 1971; Paretzke et al. 1973; Ali and Durrani 1977; Barillon et al. 1997; Nikezić 2000; Nikezić and Yu 2003; Tagami and O'Sullivan 2005; Hurford 2019). Some models describe bulk etching of anisotropic detectors using distinct etch rates parallel (v_P) and perpendicular (v_N) to the surface (Wagner 1969; Somogyi and Szalay 1973; Somogyi 1980; Durrani and Bull 1987; Sawamura and Yamazaki 1994; Ditlov 1995) or parallel and perpendicular to the ***c***-axis (Gleadow 1981). Others inferred bulk etch rates from the etched-track geometries (Masumoto 1992; Yamada et al. 1993; Villa et al. 1995; 1997; 1999).

These studies do not provide a unified model of fission-track etching in minerals and all fail on three counts: (1) none explains the qualitative difference between pitted, scratched and textured surfaces (Gleadow 1978; Jonckheere and Van den haute 1996); (2) none accounts for the different track geometries in different faces, e.g., in the basal and prism faces of apatite (Baumhauer 1875; 1887; Mehmel 1932; Jongebloed et al. 1973); (3) none predicts the basic dual structure of etched tracks, consisting of an etch pit and a channel, most obvious in pitted surfaces. We reintroduce a model owed to Gross (1918), show that it accounts for these core properties, use it to predict etched-track profiles in apatite, and compare them with observations. We conclude with some practical implications of etch-rate measurements and calculations of the true etch times of confined fission tracks.

HISTORICAL DEVELOPMENT

Fission-track etching is a specific instance of chemical etching, which falls under crystal growth and dissolution[1]. This subject has interested scientists for two centuries. Before the diffraction methods of M. von Laue and W. and L. Bragg exposed their internal structures, the understanding of crystals rested on their external properties. At the beginning of the nineteenth century, F. Mohs published observations on the dissolution of rock salt and A. von Widmanstätten on etching of iron meteorites. Daniell (1816) is credited with the first systematic investigation of crystal dissolution, noting that *"the surface of a body is never equally acted upon by a solvent"*. Brewster (1837) proposed to use the patterns of light reflected from etched surfaces for investigating their symmetries, observing that

[1] For convenience, we do not distinguish between etching and dissolution.

Always consult and cite the final, published document. See http:/www.minsocam.org or GeoscienceWorld

"different solvents ... produce different figures". Lavizzari (1865) first studied the evolving shapes of single-crystal spheres during dissolution. These innovations prompted comprehensive investigations. Goldschmidt and Wright (1903) listed 153 papers by 75 different authors, published since that of Daniell (1816).

Etching had practical significance as "*A new method for investigating the structure and composition of crystals*" (Leydolt 1855). According to Baumhauer (1894), "*the etching method allows to distinguish all 32 crystal classes and is considered superior to optical methods*". It proved to be most useful for investigating twinned, merohedral and enantiomorphic forms, as recently shown by Hejl (2017a, b) and Hejl and Finger (2018) with reference to fission-track etching in nepheline. Becke (1890) and Baumhauer (1894) summarized the results of earlier studies and formulated empirical principles still relevant to modern investigations of fission-track etching in apatite, titanite and zircon.

For given conditions, a crystallographic plane can be assigned a unique growth or dissolution rate v_R. As Masing (1922) proved, v_R is the rate of displacement of the whole plane parallel to itself; v_R is a vector perpendicular to the plane to which it refers. It is for this reason that bulk etch rates v_B cannot be used for anisotropic detectors. Growth and dissolution rates depend on orientation; the envelope of all v_R vectors is a surface called a growth or dissolution surface. Growth and dissolution surfaces are in general characterized by steep minima perpendicular to low-index faces, separated by broad maxima. There exists an overall correspondence between growth and dissolution but, depending on the nature and concentration of the etchant, maxima and minima can be interchanged and their relative magnitudes may also be affected. The faces with the lowest growth rates develop during crystal growth, the faces with high dissolution rates during dissolution. As a result of etching, etch pits develop at defects in slow-etching faces and hillocks on fast-etching faces.

Honess' (1927) monograph, "*The nature, origin and interpretation of the etch figures on crystals*", marks the end of the first mineral investigations based on etching, before diffraction methods took over. Well before then, scientists had begun addressing the theoretical problem of explaining the varied geometries of growing and dissolving crystals. P. Curie and J.W. Gibbs proposed that a solid in equilibrium with its fluid phase adopts an equilibrium form which minimizes the surface energy (capillary force). G. Wulff deduced from this that the growth form of a crystal should be bounded by slow-growing, low-index faces. A. Johnsen, in contrast, observed that non-equivalent faces with

Always consult and cite the final, published document. See http:/www.minsocam.org or GeoscienceWorld

This is the peer-reviewed, final accepted version for American Mineralogist, published by the Mineralogical Society of America.
The published version is subject to change. Cite as Authors (Year) Title. American Mineralogist, in press.
DOI: https://doi.org/10.2138/am-2022-8055. http://www.minsocam.org/

identical free energies exhibit different growth and dissolution rates in over- and under-saturated solutions. Gross (1918) concluded that the growth and dissolution forms are the products of kinetic factors, i.e., the relative growth and dissolution rates of the different crystal faces, and developed a kinetic-geometric dissolution model, which we apply in the following sections to fission-track etching in apatite.

Etching fell into disuse with the introduction of diffraction methods but regained interest when scientists demonstrated the correspondence between etch-pit and dislocation patterns (Amelinckx 1956). This made it a practical tool for investigating defects in semi-conductors and prompted new theoretical work, notably that of Frank (1958; 1972). Frank's topographic approach identifies the orientations of faces with their step densities per unit length. Growth and dissolution are treated as lateral motion of step trains parallel to flat, low-index faces. It follows from a conservation principle that the trajectories of surfaces of a given orientation are straight lines perpendicular to the tangent to a polar plot of the reciprocal etch rates (reluctance plot). The evolution of curved or polyhedral forms during growth and dissolution may be traced in this way. We refer the interested reader to the original publications for a fuller account. A simpler construction was proposed by Jaccodine (1962). Lacmann et al. (1974) went on to suggest that Frank's (1958; 1972) units steps are bounded by equilibrium form faces, thus establishing a relationship between the growth and dissolution forms of a crystal and its equilibrium form (Heimann 1975). Dissolution of apatite is of continuing interest to medical and dental research, agriculture, and to the manufacture of micro-components.

GROSS' KINETIC MODEL

Apatite etching in nitric acid is a unidirectional, non-equilibrium process (e.g., Chaïrat et al. 2007). In this case, dissolution is not defect-assisted but controlled by the intrinsic apatite etch rates (v_R), except along the tracks (v_T). We assume that neither is limited by diffusion in a stirred solution. This reduces track etching to a kinetic-geometric problem. We side-step Frank's (1972) method, because we do not aim to trace the evolution of a track through the etching process, but to predict its contour at the end. This can be achieved with Gross' (1918) older but simpler method, also described in several later publications (e.g., Masing 1922; Yamamoto 1961; Heimann 1975; Prywer 2005).

The core assumption is that, for given conditions, v_R is a fixed property of a crystallographic plane,

Always consult and cite the final, published document. See http:/www.minsocam.org or GeoscienceWorld

i.e., its rate of perpendicular displacement. Figure 1a illustrates the unit step applied to each point on the surface of a dissolving solid to obtain its form after an etch time t_E: (1) draw a tangent to the surface; (2) measure a distance $d_E = v_R\, t_E$ perpendicular to the tangent; (3) draw a parallel to the first tangent at the end of d_E; this is a tangent to the etched form, unless it has been eliminated. Elimination is a consequence of competitive dissolution of adjoining faces. Wulff (1901) explained the elimination of faces of a growing convex form, but the same principle applies to the dissolution of a concave form, such as a confined fission track. Figure 1b, after Wulff (1901) and Alexandru (1969), illustrates this principle: two faces, $F_0(a_0\text{-}c_0)$ and $G_0(c_0\text{-}e_0)$, at an external angle θ, limit a dissolving concave form (a_0-c_0-e_0). Etching for a unit etch time at rates v_F and v_G advances $F_0(a_0\text{-}c_0)$ parallel to itself to $F_1(a_1\text{-}c_1)$ and $G_0(c_0\text{-}e_0)$ to $G_1(c_1\text{-}e_1)$, creating an extra section (b_1-c_1-d_1). F and G both increase in lateral extent if their intersection c_1 lies in the sector θ (b_1-c_0-d_1); ΔF = (b_1-c_1) and ΔG = (c_1-d_1):

$$\Delta F = \frac{v_G - v_F \cos\theta}{\sin\theta} \qquad (1)$$

$$\Delta G = \frac{v_F - v_G \cos\theta}{\sin\theta} \qquad (2)$$

If c_1 does not lie in the sector θ (b_1-c_0-d_1), then F grows at the expense of G if $v_F < v_G \cos\theta$ (Figure 1b, c_0-b_0-d_1), or G grows at the expense of F if $v_G < v_F \cos\theta$ (Figure 1b, c_0-d_0-b_1). Figure 2, after Masing (1922), depicts consecutive dissolution stages of a concave polygonal initial form $F_0(a_0\text{-}b_0\text{-}c_0\text{-}d_0\text{-}e_0\text{-}f_0)$. Its faces are perpendicular to the etch-rate minima, and able to withstand the encroachment of vicinal faces with much higher etch rates. However, the polygon faces compete among themselves and (b-c) and (d-e), with somewhat higher etch-rate minima, lose out to (a-b), (c-d) and (e-f). When etching has advanced to $F_1(a_1\text{-}c_1\text{-}d_1\text{-}f_1)$, (b-c) and (d-e) have been eliminated from the dissolving form. It is worth noting that (c-d) grows at the expense of (b-c) and (d-e) up to F_1, but thereafter shrinks because it cannot hold its own against the slowest-etching faces (a-b) and (e-f).

Figure 3 illustrates Gross' (1918) method applied to circular forms. The quadrants shown present all orientations over a 90° angle to the etchant. The etch-rate plots show the etch rates parallel to an apatite prism face as a function of the ***c***-axis angle (Aslanian et al. 2021). Figures 3a-c refer to a concave initial form (F_0), e.g., a cross-section through a cylindrical hole perpendicular to the ***c***-axis. As in Figure 1a, each T-shape represents the parallel displacement of a surface section over a

Always consult and cite the final, published document. See http:/www.minsocam.org or GeoscienceWorld

distance proportional to the perpendicular etch rate. The envelope of the displaced surface sections defines the etch stage F_1. The steep etch-rate minimum parallel to ***c*** enlarges the basal face at the expense of neighbouring orientations. The less pronounced minimum perpendicular to ***c*** has a less extreme but similar effect. In Figure 3b, a second, identical etch step is applied to F_1, giving F_2; the basal and prism faces expand further so that little remains of the initial circular cross-section. This illustrates that concave forms come to be bounded by low-index faces perpendicular to the etch-rate minima, an empirical fact established before Becke (1890). Figure 3c shows that a single etch step with the combined etch action of the first ($F_0 \rightarrow F_1$) and second ($F_1 \rightarrow F_2$) gives the same result ($F_0 \rightarrow F_2$). This illustrates that a superposition principle applies to Gross' (1918) construction. This means that we can obtain etched-track shapes in one step, without having to consider intervening stages. Figures 3d ($F_0 \rightarrow F_1$), 3e ($F_1 \rightarrow F_2$) and 3f ($F_0 \rightarrow F_2$) show the corresponding dissolution stages of a convex form, e.g., a solid apatite cylinder perpendicular to the ***c***-axis, etched on the outside. In contrast to the concave form, the surfaces with the highest etch rates expand at the expense of adjacent ones. The slowest-etching faces are eliminated first and edges (corners in 3D) develop opposite the etch-rate minima. In contrast to the concave form, the areas between the edges retain some curvature. This is because the etch-rate maxima are flatter than the cusp-shaped minima, in accordance with the fact that the former correspond to high-index planes and the latter to low-index planes.

SURFACE-TRACK GEOMETRIES

Figures 4 to 6 illustrate Gross' (1918) construction applied to fission-track etching, using the etch-rate data of Aslanian et al. (2021) for Durango apatite etched in 5.5 M HNO_3 at 21 °C. Figures 4a and 4b show a track intersecting a basal surface at a 60° angle; the dash-dotted line is the axis of the latent track (t-axis). The thick solid line is the calculated track profile in the plane containing the track axis and apatite ***c***-axis. The clover leaf is the envelope of the apatite etch rates in different orientations. The shaded sector spans the etch rates that are relevant to the dissolution of apatite at the surface intersection and the end of the track. It includes the etch rate perpendicular to the surface, which determines the extent of surface lowering, and the etch rates perpendicular to the track axis, which determine the rate of channel widening. The shaded sector also includes the intermediate orientations, which exist at the surface intersection and at the end of the track. These orientations have zero initial extent but expand as etching proceeds, i.e., the converse process of the elimination of faces in Figure 2. The sectors highlighted in green contribute to the final shape of

Always consult and cite the final, published document. See http:/www.minsocam.org or GeoscienceWorld

the track. At the surface intersection the faces perpendicular to the maximum etch rates advance farthest into the apatite, forming an etch pit. No single face outcompetes all its neighbours so that the etch pit walls are slightly curved. The shape of the concave track tip, in contrast, is for the most part controlled by the steep etch-rate minima perpendicular to the basal and prism planes. The latter minimum is less pronounced, which permits neighbouring slow-etching faces, highlighted in green, to produce curvature at the connection between the track channel and the terminating prism face. Figure 4b presents the calculated profile of the same track in the plane perpendicular to that of Figure 4a.

Figure 5 shows a track intersecting a prism surface at 60°. Figure 5a shows the plane perpendicular to the surface containing the t- and ***c***-axes; Figure 5b shows the track as seen along the ***c***-axis. The clover leaf in Figure 5a again represents the apatite etch rates in a prism plane. The circular etch-rate plot in Figure 5b signifies that the etch rate shows negligible dependence on orientation about the ***c***-axis. We have as yet no data on the etch rates of different prism faces, but it is reasonable to assume that all prism planes etch at a similar rate, given the uniform channel widths in a basal plane, compared to the striking variation of track width with orientation in a prism plane. The t-axis is almost perpendicular to the maximum etch rates in the prism plane (Figure 5a). Etching thus produces a broad channel, so that no etch pit can develop at the intersection with the surface (thick dashed lines). The end of the track is made up of a basal and a prism plane, which are perpendicular to the etch-rate minima. The intersection between the bounding basal plane and the channel wall is angular; that between the bounding prism plane and the opposite channel wall is rounded. These details depend on the orientation of the track and on the variation of the etch rate about the minima. Figure 5b shows that the track is caught between a pair of slow-etching prism faces. This, together with the much greater channel width in the prism plane (Figure 5a), produces the characteristic knife-blade shape.

Figure 6 shows a track perpendicular to the ***c***-axis intersecting a prism surface. Like all tracks, it is caught between a pair of prism planes (Figure 6b), and in this specific case, between a pair of basal planes as well (Figure 6a). Thus, rather than a knife-blade shape, the track channel acquires a needle shape bounded by two pairs of slow-etching faces. Because of the narrow channel, a distinct etch pit made up of planes perpendicular to the etch-rate maxima develops at the track-surface intersection. Such maxima exist in the prism plane (Figure 6a) but not perpendicular to it (Figure 6b). The etch pit can thus grow in the ***c***-axis direction but not in a perpendicular direction, conveying it the shape

Always consult and cite the final, published document. See http:/www.minsocam.org or GeoscienceWorld

of a flat funnel. In loose terms, etch pits in a prism face are two-dimensional (flat), in contrast to those in a basal surface, which are three-dimensional (Figure 4). Because of this flattened shape and because they are often encompassed in the broad etch channels, etch pits in a prism surface are less conspicuous than in a basal face, and the apatite prism face is not considered as a pitted face despite its low etch rate.

Gross' (1918) construction thus accounts for most properties of etched surface tracks in apatite, viz. their dual structure, consisting of a convex etch pit and a concave channel, and the fact that their shapes depend on the orientation of the surface and of the track (Figure 7). The shaded sectors of the etch-rate plots indicate the range of etch rates competing to form the etched track. For a dip angle θ this range spans the interval [θ - $\pi/2$, θ + $\pi/2$]. The sectors highlighted in green are the etch rates that win out and determine the shapes of the etch pit and the track ending. These are dominated by the orientations of the maximum and minimum etch rates. Gross' (1918) model does not explain the formation of pitted, scratched and textured surfaces because it assumes that, as it advances parallel to itself, a surface remains even and flat. Equations (1) and (2) nevertheless entail that etch pits form in slow-etching faces and hillocks grow on fast-etching faces (Jonckheere and Van den haute 1996). Gross' (1918) model also accounts for the knife-blade shapes of etched tracks (Figures 4-6).

CONFINED-TRACK CONTOURS

Gross' (1918) model allows us to interpret confined-track contours and to estimate their effective etch times. Figure 8a shows a characteristic track-in-track in a prism face. The end (αβ) farthest from the host track intersection (ι) is made up of sections corresponding to the etch-rate minima parallel and perpendicular to the ***c***-axis. A different termination (δε) forms at the end closest to the host track intersection due to fast-etching faces advancing from (ι). The midsection has straight sides (βγ and εη), without the least curvature resulting from a decreasing or increasing track-etch rate v_T (Fleischer et al. 1969; 1975); (βγ) and (εη) converge away from (ι); the enclosed angle (4.4°) corresponds to a ratio v_T/v_R = arctan (4.4/2) ≈ 25. For $v_R \approx 3.0$ μm min^{-1} at 69° to ***c*** (Aslanian et al. 2021), this gives $v_T \approx 75$ μm min^{-1}, within the v_T range of Aslanian et al. (2021). At this rate, it took 10 s to etch the 12.6 μm from (ι) to the end (αβ) and under 3 s from (ι) to (δ). It took 33 s to etch the track to its greatest width (t_E = ½ × 3.3 μm/3.0 μm min^{-1} = 33 s). This is 12 s less than the immersion time (t_I = 45 s), which were needed for etching down the host track and across to the

Always consult and cite the final, published document. See http:/www.minsocam.org or GeoscienceWorld

This is the peer-reviewed, final accepted version for American Mineralogist, published by the Mineralogical Society of America.
The published version is subject to change. Cite as Authors (Year) Title. American Mineralogist, in press.
DOI: https://doi.org/10.2138/am-2022-8055. http://www.minsocam.org/

confined track. It follows that etching lasted for 23 s (33 s - 10 s) at (αβ) and 30 s (33 s - 3 s) at (δ). The track-length increase is thus difficult to predict, whichever track-etch (v_T) model one favours (Masumoto 1992; Jonckheere et al. 2017; Tamer et al. 2019; Tamer and Ketcham 2020; Aslanian et al. 2021). A better understanding of track etching nevertheless permits a fuller characterization of confined tracks than just their measured lengths and orientations. The effective etch time (t_E) and position of the intersection point (ι) are relevant for estimating overetching (Laslett et al. 1984; Yamada et al. 1993).

Figure 8b shows a track at a low angle to ***c***, with straight sides which join onto short sections parallel to ***c*** (αβ and γδ) towards both ends. Its slender form makes it difficult to estimate v_T but it is possible to calculate t_E from its width (0.6 μm) and the widening rate at 8.6° to ***c*** (0.75 μm min^{-1}; Aslanian et al. 2021). This gives t_E = ½ × 0.6 μm/0.75 μm min^{-1} = 24 s. The confined track in Figure 8c illustrates the characteristic shape of tracks almost perpendicular to the ***c***-axis. The funnel on one side of the host track (ι) consists of a channel (καβ) and an etch pit bounded by the fastest-etching faces (βγ) and (κη). The funnel (γδ and εη) on the opposite side of (ι) has consumed the channel. It is difficult to determine t_E from the channel width; t_E can instead be calculated from the distances between parallel edges bounding the funnels on both sides of the host track: 3.6 μm between (βγ) and (εη), and 3.7 μm between (γδ) and (κη). For the maximum etch rate (3.05 μm min^{-1}; Aslanian et al. 2021) this corresponds to 35 - 36 s. The surviving channel section is too short and thin for estimating v_T. Moreover, v_T cannot be calculated from the angle between (βγ) and (κη) or (γδ) and (εη) either. These angles separate the maximum etch rates to either side of the ***c***-axis in the v_R plot (Aslanian et al. 2021).

Figure 8d shows a track almost perpendicular to the ***c***-axis, but with a less regular shape than that in Figure 8c. Overlaying the slowest-etching (αβ, δε) and fastest-etching (γδ, κλ) orientations reveals a diamond shape truncated by a basal face (δε). This can be understood as a consequence of the offset of the latent host track relative to the latent confined track. The growth of fast-etching funnel faces requires convex intersections. In contrast to surface tracks (Figure 6a), these exist at confined tracks to the extent that the etched host track created them. On this assumption, the effective etch time can be calculated from the perpendicular distances between (γδ) and (κλ) and between (εη) and (λμ). The result is t_E = ½ × 2.3 μm/3.05 μm min^{-1} = 23 s, i.e., 12 s less than the track in Figure 8c, consistent with the offset of the host and the confined track. Figure 8e illustrates the case of a confined track sub-parallel to a fast-etching apatite face. All straight contour sections correspond either to slow-

Always consult and cite the final, published document. See http:/www.minsocam.org or GeoscienceWorld

This is the peer-reviewed, final accepted version for American Mineralogist, published by the Mineralogical Society of America.
The published version is subject to change. Cite as Authors (Year) Title. American Mineralogist, in press.
DOI: https://doi.org/10.2138/am-2022-8055. http://www.minsocam.org/

etching faces (αβ, δε) or to fast-etching faces (βγ, εη). Its effective etch time can nevertheless be calculated as before (37 s), but v_T-estimates based on the angles between facing edges of the track contour would be invalid. The track in Figure 8f is even more problematic, and appears to offer no hold for calculating either t_E or v_T because it lacks facing channel walls (as in Figures 8a, b) and facing funnel edges (as in Figures 8c, d, e). A tentative t_E estimate is nevertheless possible; section (εη) is parallel to the track axis and does not correspond to a slow-or a fast-etching orientation. It must thus be interpreted as one side of the track channel and its distance to the track axis (0.7 μm) is half the track width. With the apatite etch rate for an 80° ***c***-axis angle (2.1 μm min^{-1}; Aslanian et al. 2021), this gives t_E = 0.7 μm/2.1 μm min^{-1} = 20 s. Although the track in Figure 8f is not exceptional, Gross' (1918) model does not explain how segment (ηκ) results from etching a straight latent fission track.

Gross' (1918) model enables us to interpret the appearances of etched confined tracks and to gain numerical data. Most tracks are straightforward but some at high ***c***-axis angles must be interpreted with care. Gross' (1918) model also casts a light on common misconceptions about track etching. Foremost that "*the shape (cross-section) of an etch pit is the manifestation of the etching velocity space (etch-rate plot) characterizing a particular track detector (and etchant)*" (Yamada et al. 1993). According to Gross (1918), a track cross-section is a concave form bounded by the slowest-etching faces. So, we cannot calculate other etch rates from the track openings (Singh et al. 1986; Barbarand et al. 2003; Ravenhurst et al. 2003). Nor can we infer apatite etch rates from the length increase of step-etched confined tracks (Laslett et al. 1984; Watt and Durrani 1985; Carlson et al. 1999; Tamer and Ketcham 2020). The roundedness of track tips is not a valid measure of etching progress because, on continued etching, the track tips come to be bounded by basal and prism faces. Earlier studies have reported that the rate of increase of the confined-track length does not correspond to the etch rate estimated from the track openings (Masumoto 1992; Yamada et al. 1993; Ravenhurst et al. 2003). On the basis of meticulous single-track step-etch experiments Yamada et al. (1993) interpreted rounded track ends in zircon as due to a decrease of the track-etch rate, related to the discontinuous nature of latent tracks towards the ends of the fission-fragment ranges. Despite the support from latent-track studies (Paul and Fitzgerald 1992; Paul 1993; Li et al. 2011; 2012) and step-etch experiments (Jonckheere et al. 2017; Aslanian et al. 2021), this fact is still underappreciated, given that the rate of track-length increase is most important for deciding on an etch protocol (Tamer et al. 2019).

Always consult and cite the final, published document. See http:/www.minsocam.org or GeoscienceWorld

This is the peer-reviewed, final accepted version for American Mineralogist, published by the Mineralogical Society of America.
The published version is subject to change. Cite as Authors (Year) Title. American Mineralogist, in press.
DOI: https://doi.org/10.2138/am-2022-8055. http://www.minsocam.org/

Figure 9 illustrates that the surface-track openings and channels, and the confined-track contours, are all made up of straight sections. Following a 15 s etch step from 30 s to 45 s immersion, each straight edge has moved parallel to itself over a perpendicular distance which depends on its orientation, as Gross (1918) demanded. The fast-etching sides of the funnel at the intersection of the confined track with the host track expand at the expense of the slow-etching faces flanking the channel (Figure 1b). D_{PAR} increases 1.6 µm (4.0 to 5.6 µm) during 15 s etching, while the confined-track channel widens 0.2 µm (0.2 to 0.5 µm) in the same direction. One D_{PER} increases 0.4 µm (1.0 to 1.4 µm), comparable to the increase of the confined-track length in the same direction (0.5 µm), another however 1.1 µm (1.9 to 3.0 µm). This illustrates that D_{PER} (and D_{PAR}; Murrell et al. 2009; Sobel and Seward 2010; Jonckheere et al. 2020) exhibits variation from track to track. Thus neither D_{PER} or D_{PAR} represent the apatite etch rate in the direction in which they are measured. The break between the confined-track funnel and channel shifted along the track during the 15 s etch step. These features are therefore not related to unetchable gaps in the middle of the track (Hejl 1995). The curvature at both ends of the confined track is similar after 30 s immersion, but dissimilar after 45 s. The roundedness of the track ends is thus not a unique or valid measure of its etching progress. In the 15 s between 30 s and 45 s immersion, the distance between parallel sections of the funnels at the intersection of the confined track with the host track almost doubles, from 1.8 µm to 3.5 µm (Figure 9). This means that the track was in fact etched for a little over 15 s after 30 s immersion. With the etch-rates of Aslanian et al. (2021) we calculate an effective etch time t_E = 18 s and an average rate of length increase v_L = 2 µm min^{-1}. Using this approach we can also calculate t_E and v_L for other confined tracks (Aslanian et al. 2021).

IMPLICATIONS

Fission-track etching is often referred to as track revelation, in the sense of exposing something hidden from view. It is usually considered an inconsequential step in the preparation of samples for dating and (T,t)-modelling. From their formation, fission tracks are complex and varied structures onto which their thermal histories are imprinted in the form of structural modifications. Etching leaves little more than a cavity of a given shape and dimensions. Gross' (1918) etch model predicts that on continued etching the track contours come to reflect the minimum and maximum apatite etch rates. At the same time, and in contrast to isotropic detectors, all trace of the track-etch rate v_T, and with it of the latent-track structure, is lost. Fission-track etching is therefore far from inconsequential, and it is important to understand the etching process for interpreting track-

Always consult and cite the final, published document. See http:/www.minsocam.org or GeoscienceWorld

length data.

We described Gross' (1918) kinetic dissolution model, applied it to fission-track etching in apatite and showed that the results agree with microscopic observations. In principle, their effective etch times t_E and rates of length increase v_L allow us to normalize confined-track lengths to a reference etch time. We can in this manner reduce the scatter of track-length data although most of it is due to uranium fission and track formation (Wagemans 1991; Ziegler et al. 1985). Measuring the length increase of fossil tracks can be useful if v_L reflects the order in which tracks formed, i.e., if older tracks have lower v_L than younger tracks (Jonckheere et al. 2017). However, calculating v_L involves two etch steps because it differs from track to track (Aslanian et al. 2021). It therefore seems more practical to settle for a t_E estimate based on a single step if the apatite etch rates v_R are known. This would permit the setting of an etch-time window and modelling of confined track data in the selected interval. For a well-chosen window, the excluded lengths will be those of the least-etched and most-etched tracks. This numerical loss is offset by the fact that an etch-time window eliminates the need to control the immersion time. A longer immersion time brings a rapid increase of the number of measurable confined tracks, including ones within the etch-time window (Ito 2004; Jonckheere et al. 2007). Apart from the immersion time, the proposed method requires no changes to existing procedures if an appropriate window can be defined for each protocol so as to give consistent results. This is, in our opinion, not problematic for common protocols that are not too different to start with (Tamer et al. 2019). We expect that track-length data for apatites with different chemical compositions will become more uniform if their etch-time windows are linked to D_{PAR} or another compositional indicator (Carlson et al. 1999; Barbarand et al. 2003). In the ideal case, this could make compositional annealing corrections redundant. It is however essential for the acceptance of the proposed method that it be based on more extensive experimental data.

ACKNOWLEDGMENT AND FUNDING

This research was funded by the German Research Council (DFG project Jo 358/4-1). The authors are pleased to acknowledge the efficient editorial handling by Fang-Zhen Teng, and the constructive professional reviews of Róbert Arató and Andrew J.W. Gleadow, which considerably improved the manuscript.

Always consult and cite the final, published document. See http:/www.minsocam.org or GeoscienceWorld

This is the peer-reviewed, final accepted version for American Mineralogist, published by the Mineralogical Society of America.
The published version is subject to change. Cite as Authors (Year) Title. American Mineralogist, in press.
DOI: https://doi.org/10.2138/am-2022-8055. http://www.minsocam.org/

REFERENCES CITED

Alexandru, H.V. (1969) A macroscopic model for the habit of crystals grown from solutions. Journal of Crystal Growth, 5, 115-124.

Ali, A., and Durrani, S.A. (1977) Etched-track kinetics in isotropic detectors. Nuclear Track Detection, 1, 107-121.

Amelinckx, S. (1956) The direct observation of dislocation nets in rock salt single crystals. Philosophical Magazine, 8, 269-290.

Aslanian, C., Jonckheere, R., Wauschkuhn, B., and Ratschbacher, L. (2021) A quantitative description of fission-track etching in apatite. American Mineralogist, 106, in press.

Barbarand, J., Hurford, T., and Carter, A. (2003) Variation in apatite fission-track length measurement: implications for thermal history modelling. Chemical Geology, 19, 77-106.

Barillon, R., Fromm, M., Chambaudet, A., Marah, H., and Sabir, A. (1997) Track etch velocity study in a radon detector (LR 115, cellulose nitrate). Radiation Measurements, 28, 619-628.

Baumhauer, H. (1875) On the etch figures of apatite and gypsum. Sitzungsberichte der mathematisch-physikalischen Classe der königlichen Bayerischen Akademie der Wissenschaften zu München, 5, 169-177 (in German).

Baumhauer, H. (1887) On the dependence of apatite etch figures on the nature and concentration of the etchant. Sitzungsberichte der königlichen Preussischen Akademie der Wissenschaften zu Berlin, 42, 863-878 (in German).

Baumhauer, H. (1894) Results of the etch method in crystallographic research. Wilhelm Engelmann Verlag, Leipzig, pp. 131 + 12 plates (in German).

Becke, F. (1890) Etch experiments on fluorite. Tschermaks Mineralogische und Petrographische Mitteilungen, 424, 349-437 + 1 plate (in German).

Bhandari, N., Bhat, S.G., Lal, D., Rajagopalan, G., Tamhane, A.S.J., and Venkatavaradan, V.S. (1971) Fission fragment tracks in apatite: recordable track lengths. Earth and Planetary Science Letters, 13, 191-199.

Brewster, D. (1837) On the optical figures produced by the disintegrated surfaces of crystals. The London, Edinburgh, and Dublin Philosophical Magazine and Journal of Science, 5, 16-28 + 5 plates.

Carlson, W.D., Donelick, R.A., and Ketcham, R.A. (1999) Variability of apatite fission-track annealing kinetics: I. Experimental results. American Mineralogist, 84, 1213-1223.

Chaïrat, C., Schott, J., Oelkers, E.H., Lartigue, J.-E., and Harouiya, N. (2007) Kinetics and mechanism of natural fluorapatite dissolution at 25 °C and pH from 3 to 12. Geochimica et Cosmochimica Acta, 71, 5901-5912.

Crowley, K.D., Cameron, M., and Schaeffer, L. (1991) Experimental studies on annealing of etched fission tracks in fluorapatite. Geochimica et Cosmochimica Acta, 55, 1449-1465.

Daniell, F., (1816) On some phenomena attending the process of solution, and on their application to the laws of crystallization. The Quarterly Journal of Science and the Arts, edited at the Royal Institution of Great

Always consult and cite the final, published document. See http:/www.minsocam.org or GeoscienceWorld

This is the peer-reviewed, final accepted version for American Mineralogist, published by the Mineralogical Society of America.
The published version is subject to change. Cite as Authors (Year) Title. American Mineralogist, in press.
DOI: https://doi.org/10.2138/am-2022-8055. http://www.minsocam.org/

Britain, 1, 24-49 + 3 plates.

Ditlov, V. (1995) Calculated tracks in plastics and crystals. Radiation Measurements, 25, 89-94.

Durrani, S.A., and Bull, R.K. (1987) Solid state nuclear track detection. Principles, methods and applications. Pergamon Press, Oxford, pp. 304.

Fleischer, R.L., and Price, P.B. (1964) Techniques for geological dating of minerals by chemical etching of fission fragment tracks. Geochimica et Cosmochimica Acta, 28, 1705-1714.

Fleischer, R.L., Price, P.B., and Walker, R.M. (1975) Nuclear tracks in solids. Principles and applications. University of California Press, Berkeley; pp. 604.

Fleischer, R.L., Price, P.B., and Woods, R.T. (1969) Nuclear particle track identification in inorganic solids. Physical Review, 88, 563-567.

Frank, F.C. (1958) On the kinematic theory of crystal growth and dissolution processes. In T.H. Doremus, B.W. Roberts, and D. Turnbull, Eds., Growth and perfection of crystals, Wiley, p. 411-419.

Frank, F.C. (1972) On the kinematic theory of crystal growth and dissolution processes, II. Zeitschrift für Physikalische Chemie Neue Folge, 77, 84-92.

Gleadow, A.J.W. (1978) Anisotropic and variable track etching characteristics in natural sphenes. Nuclear Track Detection, 2, 105-111.

Gleadow, A.J.W. (1981) Fission track dating methods: what are the real alternatives? Nuclear Tracks, 5, 3-14.

Gleadow, A.J.W., and Lovering, J.F. (1977) Geometry factor for external detectors in fission track dating. Nuclear Track Detection, 1, 99-106.

Goldschmidt, V., and Wright, F.E. (1903) On etch figures, light figures and dissolution forms, with observations on calcite. Neues Jahrbuch für Mineralogie, Geologie, Paläontologie, Beilage Band, 17, 355-390 (in German).

Green, P.F., Duddy, I.R., Gleadow, A.J.W., Tingate, P.R., and Laslett, G.M. (1986) Thermal annealing of fission tracks in apatite 1. A qualitative description. Chemical Geology (Isotope Geoscience Section), 59, 237-253.

Green, P.F., and Durrani, S.A. (1978) A quantitative assessment of geometry factors for use in fission track studies. Nuclear Track Detection, 2, 207-213.

Gross, R. (1918) On the theory of growth and dissolution processes of crystalline matter. Abhandlungen der mathematisch-physischen Klasse der königlichen Sächsischen Gesellschaft der Wissenschaften zu Leipzig, 35, 137-202 (in German).

Heimann, R.B. (1975) Dissolution of crystals. Theory and practical application. Applied Mineralogy, 8, Springer, pp. 270 (in German).

Hejl, E. (1995) Evidence for unetchable gaps in apatite fission tracks. Chemical Geology (Isotope Geoscience Section), 122, 259-269.

Hejl, E. (2017a) Are fission tracks in enantiomorphic minerals a key to the emergence of homochirality? Neues Jahrbuch für Mineralogie Abhandlungen, 194, 97-106.

Always consult and cite the final, published document. See http:/www.minsocam.org or GeoscienceWorld

Hejl, E. (2017b) First observation of etched uranium fission tracks in nepheline by Hermann Traube (1895)? Mitteilungen der Österreichische Mineralogische Gesellschaft, 162, 83-90.

Hejl, E., and Finger, F. (2018) Chiral proportions of nepheline originating from low-viscosity alkaline melts. A pilot study. Symmetry, 10, 410.

Henke, R.P., and Benton, E.V. (1971) On geometry of tracks in dielectric nuclear track detectors. Nuclear Instruments and Methods, 9, 483-489.

Holmes, P.J. (1962) Practical applications of chemical etching. In P.J. Holmes, Ed., The Electro-Chemistry of Semiconductors, p. 329-377. Academic Press.

Honess, A.P. (1927) The nature, origin and interpretation of the etch figures on crystals. Wiley, New York, pp. 171.

Hurford, A.J. (1990a) Standardization of fission track dating calibration. Recommendation by the Fission Track Working Group of the I.U.G.S. Subcomission on Geochronology. Chemical Geology (Isotope Geoscience Section), 80, 171-178.

Hurford, A.J. (1990b) International Union of Geological Sciences subcommission on geochronology recommendation for the standardization of fission track dating calibration and data reporting. Nuclear Tracks and Radiation Measurements, 17, 233-236.

Hurford, A.J. (2019) An historical perspective on fission-track thermochronology. In M.G. Malusà and P.G. Fitzgerald, Eds., Fission-Track Thermochronology and its Application to Geology, Geography and Environment, p. 3–23. Springer.

Ito, H. (2004) On a simple approach to increase TINT numbers in apatite. Fission Track News Letter, 17, 1-7 (in Japanese with English abstract).

Jaccodine, R.J. (1962) Use of modified free energy theorems to predict equilibrium growing and etching shapes. Journal of Applied Physics 33, 2643–2647.

Jafri, E.H., Qureshi, A.A., Sial, M.A., and Khan, H.A. (1990) Track shapes, etching characteristics and track density distribution on different planes of apatite. Radiation Effects and Defects in Solids, 115, 227-232.

Jonckheere, R. (2003) On the densities of etchable fission tracks in a mineral and co-irradiated external detector with reference to fission-track dating of minerals. Chemical Geology, 200, 41-58.

Jonckheere, R., Aslanian, C., Wauschkuhn, B., and Ratschbacher, L. (2020) Some geometrical properties of fission-track-surface intersections in apatite. American Mineralogist, 105, 1355-1364.

Jonckheere, R., Enkelmann, E., Min, M., Trautmann, C., and Ratschbacher, L. (2007) Confined fission tracks in ion-irradiated and step-etched prismatic sections of Durango apatite. Chemical Geology, 242, 202–217.

Jonckheere, R., Enkelmann, E., and Stübner, K. (2005) Observations on the geometries of etched fission and alpha-recoil tracks with reference to models of track revelation in minerals. Radiation Measurements 39, 577-583.

Jonckheere, R., Tamer, M.T., Wauschkuhn, B., Wauschkuhn, F., and Ratschbacher, L. (2017) Single-track length measurements of step-etched fission tracks in Durango apatite: "Vorsprung durch Technik". American

Always consult and cite the final, published document. See http:/www.minsocam.org or GeoscienceWorld

This is the peer-reviewed, final accepted version for American Mineralogist, published by the Mineralogical Society of America.
The published version is subject to change. Cite as Authors (Year) Title. American Mineralogist, in press.
DOI: https://doi.org/10.2138/am-2022-8055. http://www.minsocam.org/

Mineralogist, 102, 987–996.

Jonckheere, R., and Van den haute, P. (1996) Observations on the geometry of etched fission tracks in apatite: implications for models of track revelation. American Mineralogist, 81, 1476-1493.

Jonckheere, R., Wauschkuhn, B., and Ratschbacher, L. (2019) On growth and form of etched fission tracks in apatite: A kinetic approach. American Mineralogist, 104, 569-579.

Jongebloed, W.L., Molenaar, I., and Arends, J. (1973) Orientation-dependent etchpit penetration and dissolution of fluorapatite. Caries Research, 7, 154-165.

Krishnaswami, S., Lal, D., Prabhu, N., and Macdougall, D. (1974) Characteristics of fission tracks in zircon: Applications to geochronology and cosmology. Earth and Planetary Science Letters, 22, 51-59.

Lacmann, R., Franke, W., and Heimann, R. (1974) The dissolution forms of single crystal spheres. I. Theory for the molecular-kinetics interpretation. Journal of Crystal Growth, 26, 107-116.

Laslett, G.M., Gleadow, A.J.W., and Duddy, I. (1984) The relationship between fission track length and track density in apatite. Nuclear Tracks, 9, 29-38.

Lavizzari, L. (1865) New phenomena of crystalline bodies. Imprimerie et Lithographie Cantonale, Lugano, pp. 54 + 14 plates (in French).

Leydolt, F. (1855) On a new method for investigating the structure and composition of crystals. Sitzungsberichte der kaiserliche Academie der Wissenschaften, Vienna, 15, pp. 59 + 5 plates (in German).

Li, W., Kluth, P., Schauries, D., Rodriguez, M.D., Lang, M., Zhang, F., Zdorovets, M., Trautmann, C., and Ewing, R.C. (2014) Effect of orientation on ion track formation in apatite and zircon. American Mineralogist, 99, 1127-1132.

Li, W., Lang, M., Gleadow, A.J.W., Zdorovets, M.V., and Ewing, R.C. (2012) Thermal annealing of unetched fission tracks in apatite. Earth and Planetary Science Letters, 321-322, 121-127.

Li, W., Wang, L., Lang, M., Trautmann, C., and Ewing, R.C. (2011) Thermal annealing mechanisms of latent fission tracks: Apatite *vs*. zircon. Earth and Planetary Science Letters, 302, 227-235.

Masing, G. (1922) Growth and dissolution of crystals. Die Naturwissenschaften, 41, 899-908 (in German).

Masumoto, S. (1992) Etching characteristics of zircon in fission track dating. Journal of Geosciences, Osaka City University, 35, 13-31.

Mehmel, M. (1932) Relationships between crystal structure and chemical formula of apatite. Zeitschrift Für Physikalische Chemie, 15B, 223-241 (in German).

Moreira, P.A.F.P., Guedes, S., Iunes, P.J., and Hadler, J.C. (2010) Fission track chemical etching kinetic model. Radiation Measurements, 45, 157–162.

Murrell, G.M., Sobel, E.R., Carrapa, B., and Andriessen, P. (2009) Calibration and comparison of etching techniques for apatite fission-track thermochronology. In Lisker, F., Ventura, B., and Glasmacher, U.A., Eds., Thermochronological Methods: From Palaeotemperature Constraints to Landscape Evolution Models. Geological Society, London, Special Publications, 324, 73–8.

Always consult and cite the final, published document. See http:/www.minsocam.org or GeoscienceWorld

This is the peer-reviewed, final accepted version for American Mineralogist, published by the Mineralogical Society of America.
The published version is subject to change. Cite as Authors (Year) Title. American Mineralogist, in press.
DOI: https://doi.org/10.2138/am-2022-8055. http://www.minsocam.org/

Naeser, C.W. (1967) The use of apatite and sphene for fission track age determinations. Bulletin of the Geological Society of America, 78, 1523-1526.

Nikezić, D. (2000) Three dimensional analytical determination of the track parameters. Radiation Measurements, 32, 277-282.

Nikezić, D., and Yu, K.N. (2003) Three-dimensional analytical determination of the track parameters: overetched tracks. Radiation Measurements, 37, 39-45.

Paretzke, H.G., Benton, E.V., and Henke, R.P. (1973) On particle track evolution in dielectric track detectors and charge identification through track radius measurement. Nuclear Instruments and Methods, 108, 73-80.

Patel, A.R., Agarwal, M.K., and Desai, C.C. (1967) Fission tracks on (10-10) cleavages of natural apatite crystals. Journal of the Physical Society of Japan, 23, 553-555.

Paul, T.A. (1993) Transmission electron microscopy investigation of unetched fission tracks in fluorapatite - physical process of annealing. Nuclear Tracks and Radiation Measurements, 21, 507-511.

Paul, T.A., and Fitzgerald, P.G. (1992) Transmission electron microscopic investigation of fission tracks in fluorapatite. American Mineralogist, 77, 336-344.

Poupeau, G., Carpéna, J., Mailhé, D., and Ceylan, V.K. (1980) Isothermal plateau ages in the fission track dating method. Comptes Rendus de l'Académie des Sciences de Paris D, 290, 1189-1192 (in French).

Prywer, J. (2005) Kinetic and geometric determination of the growth morphology of bulk crystals: Recent developments. Progress in Crystal Growth and Characterization of Materials, 50, 1-38.

Ravenhurst, C.E., Roden-Tyce, M.K., and Miller, D.S. (2003) Thermal annealing of fission tracks in fluorapatite, chlorapatite, manganoanapatite, and Durango apatite: experimental results. Canadian Journal of Earth Science, 40, 995-1007.

Sandhu, A.S., Singh, S., and Virk, H.S. (1988a) Anisotropic etching and annealing studies of fission tracks in zircon. Nuclear Tracks and Radiation Measurements, 15, 245-247.

Sandhu, A.S., Singh, S., and Virk, H.S. (1988b) The effect of anisotropic track etching and annealing on fission track age determination in minerals. Nuclear Tracks and Radiation Measurements, 15, 723-725.

Sawamura, T., and Yamazaki, H. (1994) Development of etched tracks in anisotropic solid. Radiation Effects and Defects in Solids, 132, 57-66.

Singh, S., Singh, D., Sandhu, A.S., and Virk, H.S. (1986) A study of etched track anisotropy in apatite. Mineralogical Journal, 13, 75-85.

Sobel, E.R., and Seward, D. (2010) Influence of etching conditions on apatite fission-track etch pit diameter. Chemical Geology, 271, 59-69.

Somogyi, G. (1980) Development of etched nuclear tracks. Nuclear Instruments and Methods, 173, 21-42.

Somogyi, G., and Szalay, S.A. (1973) Track-diameter kinetics in dielectric track detectors. Nuclear Instruments and Methods, 109, 211-232.

Always consult and cite the final, published document. See http:/www.minsocam.org or GeoscienceWorld

This is the peer-reviewed, final accepted version for American Mineralogist, published by the Mineralogical Society of America.
The published version is subject to change. Cite as Authors (Year) Title. American Mineralogist, in press.
DOI: https://doi.org/10.2138/am-2022-8055. http://www.minsocam.org/

548 Tagami, T., and O'Sullivan, P.B. (2005) Fundamentals of fission-track thermochronology. Reviews in
549 Mineralogy and Geochemistry, 58, 19-47.

550 Tamer, M.T., Chung, L., Ketcham, R.A., and Gleadow, A.J.W. (2019) Analyst and etching protocol effects on the
551 reproducibility of apatite confined fission-track length measurement, and ambient-temperature annealing
552 at decadal timescales. American Mineralogist, 104, 1421-1435.

553 Tamer, M.T., and Ketcham, R.A. (2020) The along-track etching structure of fission tracks in apatite:
554 Observations and implications. Chemical Geology, 553, 119809.

555 Tello, C.A., Palissari, R., Hadler, J.C., Iunes, P.J., Guedes, S., Curvo, E.A.C., and Paulo, S.R. (2006) Annealing
556 experiments on induced fission tracks in apatite: Measurements of horizontal-confined track lengths and
557 track densities in basal sections and randomly oriented grains. American Mineralogist, 91, 252–260.

558 Villa, F., Grivet, M., Rebetez, M., Dubois, C., and Chambaudet, A. (1995) Modeling the fission track etching
559 process in apatite: segmentation or crystallography influence. Radiation Measurements, 25, 137-140.

560 Villa, F., Grivet, M., Rebetez, M., Dubois, C., and Chambaudet, A. (1997) Calibration and simulation of apatite
561 fission track etching: influence of diffusion and crystal symmetry. Radiation Measurements, 28, 543-548.

562 Villa, F., Grivet, M., Rebetez, M., Dubois, C., Chambaudet, A., Chevarier, A., Martin, P., Brossard, F., Blondiaux, G.,
563 Sauvage, T., and Toulemonde M. (1997) Damage morphology of Kr ion tracks in apatite: dependence on
564 dE/dX. Radiation Measurements, 31, 65-70.

565 Wagemans, C., Ed. (1991) The nuclear fission process. CRC Press, Inc., Boca Raton, Florida, United States of
566 America.

567 Wagner, G.A. (1969) Tracks from spontaneous ^{238}U-fission as a means for dating apatite and a contribution to
568 the geochronology of the Odenwald. Neues Jahrbuch für Mineralogie Abhandlungen, 110, 252-286 (in
569 German).

570 Watt, S., and Durrani, S.A. (1985) Thermal stability of fission tracks in apatite and sphene: using confined
571 track length measurements. Nuclear Tracks, 10, 349-357.

572 Wauschkuhn, B., Jonckheere, R., and Ratschbacher, L. (2015) The KTB apatite fission-track profiles: Building
573 on a firm foundation? Geochimica et Cosmochimica Acta, 167, 27–62.

574 Wulff, G. (1901) On the question of the growth and dissolution rate of crystal faces. Zeitschrift Für
575 Kristallographie, 34, 449-530 (in German).

576 Yamada, R., Tagami, T., and Nishimura, S. (1993) Assessment of overetching factor for fission track length
577 measurement in zircon. Chemical Geology (Isotope Geoscience Section), 104, 251-259.

578 Yamamoto, M. (1961) On the growth and dissolution shapes of spherical shell crystals and the shapes of etch
579 pits on crystals. Science Reports of the Research Institutes, Tohoku University, A, Physics, Chemistry and
580 Metallurgy, 13, 168-173.

581 Ziegler, J.F., Biersack, J.P., and Littmark, U. (1985) The stopping and range of ions in solids. Pergamon, New
582 York. 321 pp.
583

Always consult and cite the final, published document. See http:/www.minsocam.org or GeoscienceWorld

This is the peer-reviewed, final accepted version for American Mineralogist, published by the Mineralogical Society of America.
The published version is subject to change. Cite as Authors (Year) Title. American Mineralogist, in press.
DOI: https://doi.org/10.2138/am-2022-8055. http://www.minsocam.org/

584 ## FIGURE CAPTIONS

585 **Figure 1.** Construction of etched-track contours. (**a**) Unit step: each tangent to the initial form (F_0),
586 e.g., at a_0, is shifted parallel to itself over a perpendicular distance proportional to the etch time t_E
587 and etch rate v_R. The parallel face at a_1 is tangent to the etched track (F_1) if it is not eliminated by
588 etching of the faces adjacent to a_0 (Figure 2). (**b**) Etching of a concave intersection between two
589 faces. During etching, F_0 (etch rate v_F) and G_0 (etch rate v_G), intersecting at c_0, advance to F_1 and
590 G_1, intersecting at c_1. Both increase in extent if c_1 lies in the sector θ subtended by lines normal to
591 F_0 and G_0 through c_0. The dashed lines and highlighted right-angle triangles illustrate limiting
592 cases where either F_0 or G_0 neither grows nor shrinks. A numerical treatment permits the deriva-
593 tion of equations (1) and (2), defining the criteria for growth or shrinkage (modified after Wulff
594 1901, and Alexandru 1969).

595 **Figure 2.** Etching of a concave polygonal shape $F_0(a_0\text{-}\ b_0\text{-}c_0\text{-}d_0\text{-}e_0\text{-}f_0)$ with etch-rate minima v_{ab}, v_{bc},
596 v_{cd}, v_{de}, and v_{ef} perpendicular to (a_0-b_0), (b_0-c_0), (c_0-d_0), (d_0-e_0), and (e_0-f_0). Due to its lower etch rate
597 (v_{cd}), (c_0-d_0) grows at the expense of adjacent faces (b_0-c_0) and (d_0-e_0) with somewhat higher etch
598 rates (v_{bc} and v_{de}). At stage $F_1(a_1\text{-}\ c_1\text{-}d_1\text{-}f_1)$, ($c_1$-$d_1$) enters in competition with (a_1-c_1) and (d_1-f_1) with
599 still lower etch rates (v_{ab} and v_{ef}). Its growth is reversed and (c_1-d_1) shrinks to (c_2-d_2) and will be
600 eliminated in time (after Masing 1922). Lower left: etch-rate plot (dissolution surface) showing the
601 etch-rate minima v_{ab}, v_{bc}, v_{cd}, v_{de}, and v_{ef}; and broad etch-rate maxima, *m*, *n*, *o*, and *p*, separating the
602 steep minima.

603 **Figure 3.** Etching of a curved surface; the etch rates are those measured as a function of ***c***-axis angle
604 in an apatite prism face etched in 5.5 M HNO_3 at 21 °C (Aslanian et al. 2021). (**a-c**) Concave circular
605 form; (**a**) first etch step starting from the initial circular quadrant (shape F_0) leading to stage F_1. F_0
606 is approximated by nineteen tangents at 5° intervals each translated proportional to the perpen-
607 dicular etch rate as indicated by the T-shapes (Figure 1a). The etched form F_1 is the inside tangent
608 to all the translated surface sections. Some fast-etching ones are cut by the slow-etching basal face
609 perpendicular to ***c***, reducing F_1 to seven of the original nineteen sections. (**b**) second, identical etch
610 step applied to F_1, resulting in F_2; (**c**) a single step with the combined etch time of $F_0 \rightarrow F_1$ and $F_1 \rightarrow F_2$
611 gives the same result as two successive steps. (**d-f**) Convex circular initial form; (**d**): first etch step
612 from F_0 to F_1; (**e**): second etch step from F_1 to F_2; (**f**): one step with the combined duration of $F_0 \rightarrow F_1$
613 and $F_1 \rightarrow F_2$. These constructions illustrate that concave forms come to be bounded by flat faces

Always consult and cite the final, published document. See http:/www.minsocam.org or GeoscienceWorld

perpendicular to the etch-rate minima, whereas edges and corners develop opposite the minima on a convex form. For clearer illustration, $F_0 \rightarrow F_1$ and $F_1 \rightarrow F_2$ each correspond to two and $F_0 \rightarrow F_2$ to four etch-time units in (**a-c**), while $F_0 \rightarrow F_1$ and $F_1 \rightarrow F_2$ correspond to one half and $F_0 \rightarrow F_2$ to one full etch-time unit in (**d-f**).

Figure 4. Profiles of a track intersecting an apatite basal face at 60°. (**a**) Plane containing the track t-axis and ***c***-axis; (**b**) plane perpendicular to (**a**) containing the ***c***-axis. The etch channel widens at the rate perpendicular to the t-axis; the shaded etch rates indicate the faces that can expand from the surface intersection and endpoint. Those highlighted in green are the faces that determine the result. This is a knife-blade shaped channel, connected to the apex of a low upside-down pyramid with somewhat curved walls. The end of the track is bounded by edges parallel to the prism and basal face.

Figure 5. Profiles of a track intersecting an apatite prism face at 60°. (**a**) Plane of the track axis and ***c***-axis; (**b**) plane perpendicular to the ***c***-axis. The channel widens at a rate close to the maximum etch rate, preventing an etch pit from developing at the surface. The track is knife-blade shaped and terminated by basal and prism faces. One side of the channel meets the basal face at an angle, while the facing side gradually joins onto the prism face. This difference is a consequence of the less pronounced etch-rate minimum perpendicular to the prism face than perpendicular to the basal face.

Figure 6. Profiles of a track intersecting an apatite prism face at 60°. (**a**) Plane of the track axis and apatite ***c***-axis; (**b**) plane perpendicular to the ***c***-axis. This track is flanked by a pair of basal faces as well as a pair of prism faces. In this case, the etch channel is not knife-blade shaped but needle (rod) shaped, allowing a distinct etch pit to develop. Because there are no pronounced etch-rate maxima or minima in the plane perpendicular to ***c***, the etch pit develops noticeably only parallel to the ***c***-axis.

Figure 7. Etched surface tracks in apatite. **(a)** transmitted-light microphotograph of tracks in a basal surface with a funnel shape, consisting of a shallow etch pit connected to a channel (dark; cf. Figure 4); the channel width shows little variation with the azimuth orientation of the track, indicating that the etch rates of the flanking prism faces are similar; the tracks indicated with an arrow have no channel because the track endpoint has been overtaken by the growth of the etch pit, which in

Always consult and cite the final, published document. See http:/www.minsocam.org or GeoscienceWorld

agreement with Gross' (1918) dissolution model develops a flat bottom parallel to the basal face; the terraced internal structure of these etch pits still reveals the orientation of the latent tracks and suggests intermittent etching at the track endpoints; (**b**) compressed transmitted-light image stack of tracks in a prism face; the yellow arrows indicate etched tracks close to perpendicular to the ***c***-axis with a funnel shape, consisting of an elongated etch pit and narrow channel (cf. Figure 6); the green arrows indicate tracks at intermediate angles to ***c***, exhibiting the characteristic knife-blade shape (cf. Figure 5); the red arrows indicate tracks at low angles to ***c***, in which the knife-blade is seen edge-on.

Figure 8. Horizontal confined fission tracks in prism faces of Durango apatite etched for 45 s in 5.5 M HNO_3 at 21 °C. (**a**) shows a track with a straight channel with subparallel sides, terminated by a basal and a prism face at one end; the opposite end has a more complex shape due to the interference of the slow-etching faces developing at the endpoint and fast-etching faces advancing from the nearby host-track intersection (ι). This does not prevent measurement of the track width (3.3 μm) close to (ι) and the taper of the track channel (4.4°), from which its effective etch time t_E and etch rate v_T can be estimated (Aslanian et al. 2021). (**b**) shows a thin track at a small angle to ***c***, for which it is difficult to measure the angle between the sides of the track channel, although measuring the track thickness is possible. (**c**)-(**f**) show tracks at angles greater than 75° to ***c***, bounded by combinations of fast-etching and slow-etching faces. Track etch rate estimates are often not possible, but, with a model-based understanding of the track-etching process, it is possible in most cases to interpret their contours, and calculate their effective etch times with adequate precision (see text). Green: slowest-etching faces; yellow: fastest-etching faces; orange: unexplained section of the track contour; all lengths are in μm, and all angles in degrees (°).

Figure 9. Surface tracks and a horizontal confined track in a prism face of Durango apatite after (**a**) 30 s and (**b**) 45 s immersion in 5.5 M HNO_3 at 21 °C. Except for the ends of the confined track, their contours are all made up of straight sections. Regardless of their changed dimensions, corresponding sections are parallel after 30 s and 45 s etching, i.e., each maintains its orientation. Their displacement varies with orientation demonstrating that the apatite etch rate is anisotropic, consistent with Gross' (1918) dissolution model. The dotted lines are the contours of the track openings and of the confined track after 45 s (**a**) and 30 s immersion (**b**); all lengths are in μm, and all angles in degrees (°).

Always consult and cite the final, published document. See http:/www.minsocam.org or GeoscienceWorld

This is the peer-reviewed, final accepted version for American Mineralogist, published by the Mineralogical Society of America.
The published version is subject to change. Cite as Authors (Year) Title. American Mineralogist, in press.
DOI: https://doi.org/10.2138/am-2022-8055. http://www.minsocam.org/

FIGURES

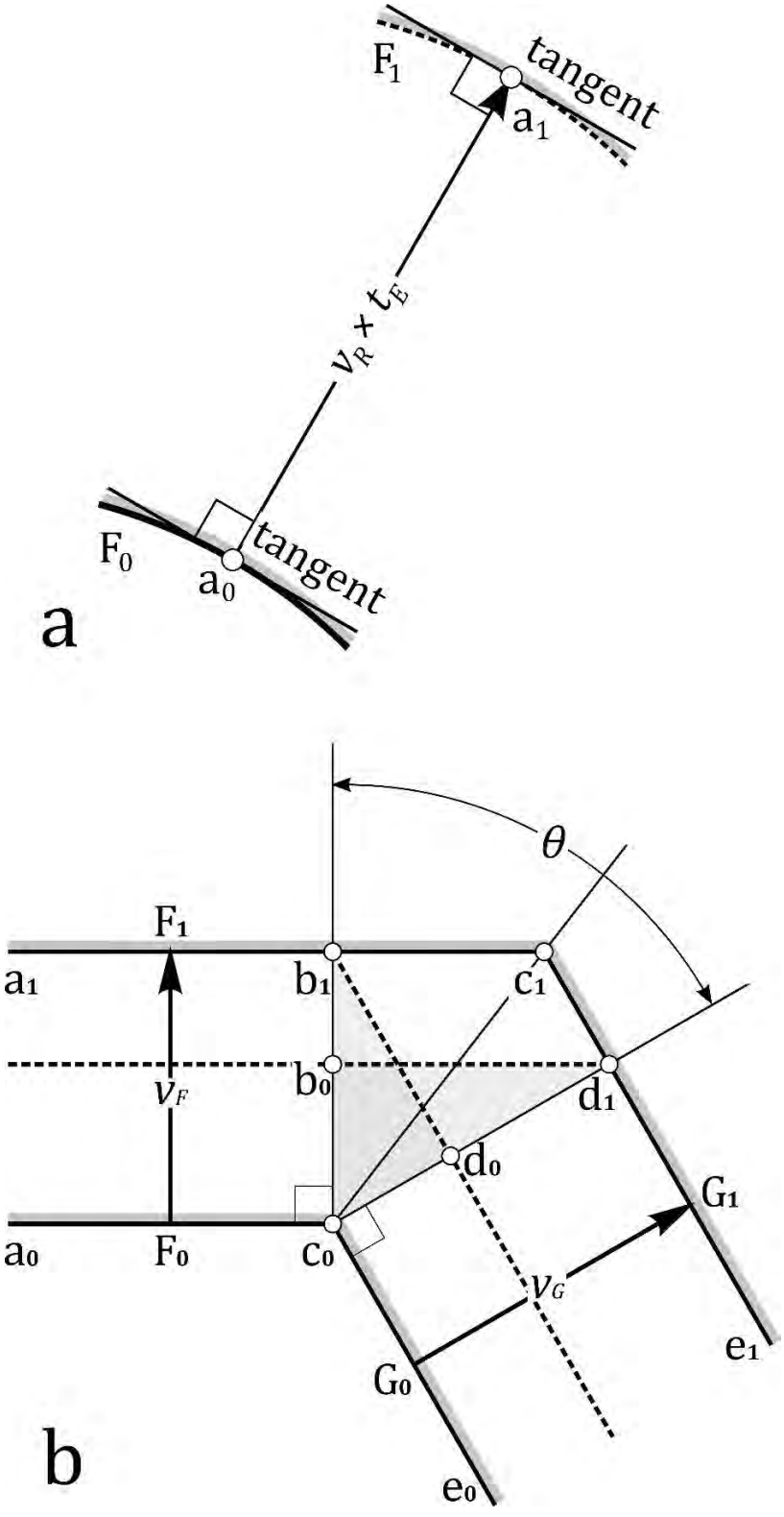

Figure 1

Always consult and cite the final, published document. See http:/www.minsocam.org or GeoscienceWorld

This is the peer-reviewed, final accepted version for American Mineralogist, published by the Mineralogical Society of America.
The published version is subject to change. Cite as Authors (Year) Title. American Mineralogist, in press.
DOI: https://doi.org/10.2138/am-2022-8055. http://www.minsocam.org/

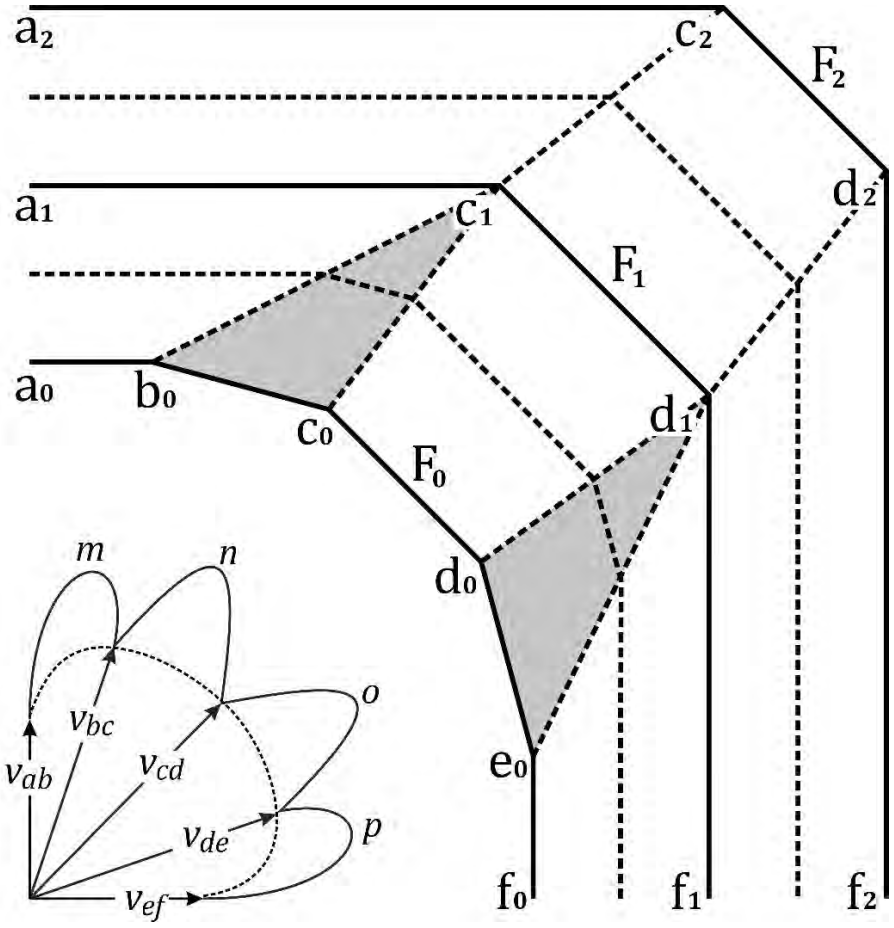

Figure 2

Always consult and cite the final, published document. See http:/www.minsocam.org or GeoscienceWorld

This is the peer-reviewed, final accepted version for American Mineralogist, published by the Mineralogical Society of America.
The published version is subject to change. Cite as Authors (Year) Title. American Mineralogist, in press.
DOI: https://doi.org/10.2138/am-2022-8055. http://www.minsocam.org/

Figure 3

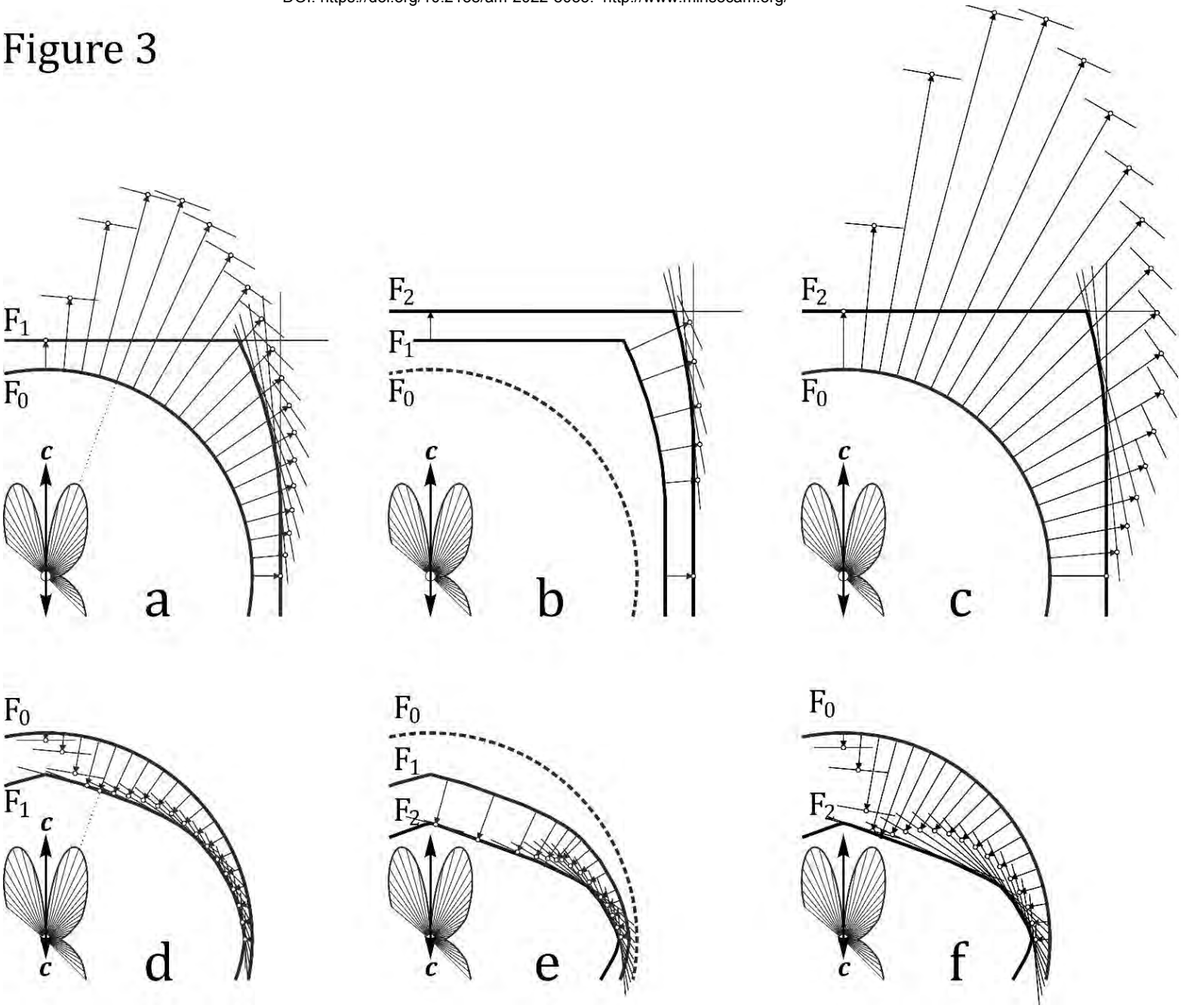

Always consult and cite the final, published document. See http:/www.minsocam.org or GeoscienceWorld

This is the peer-reviewed, final accepted version for American Mineralogist, published by the Mineralogical Society of America.
The published version is subject to change. Cite as Authors (Year) Title. American Mineralogist, in press.
DOI: https://doi.org/10.2138/am-2022-8055. http://www.minsocam.org/

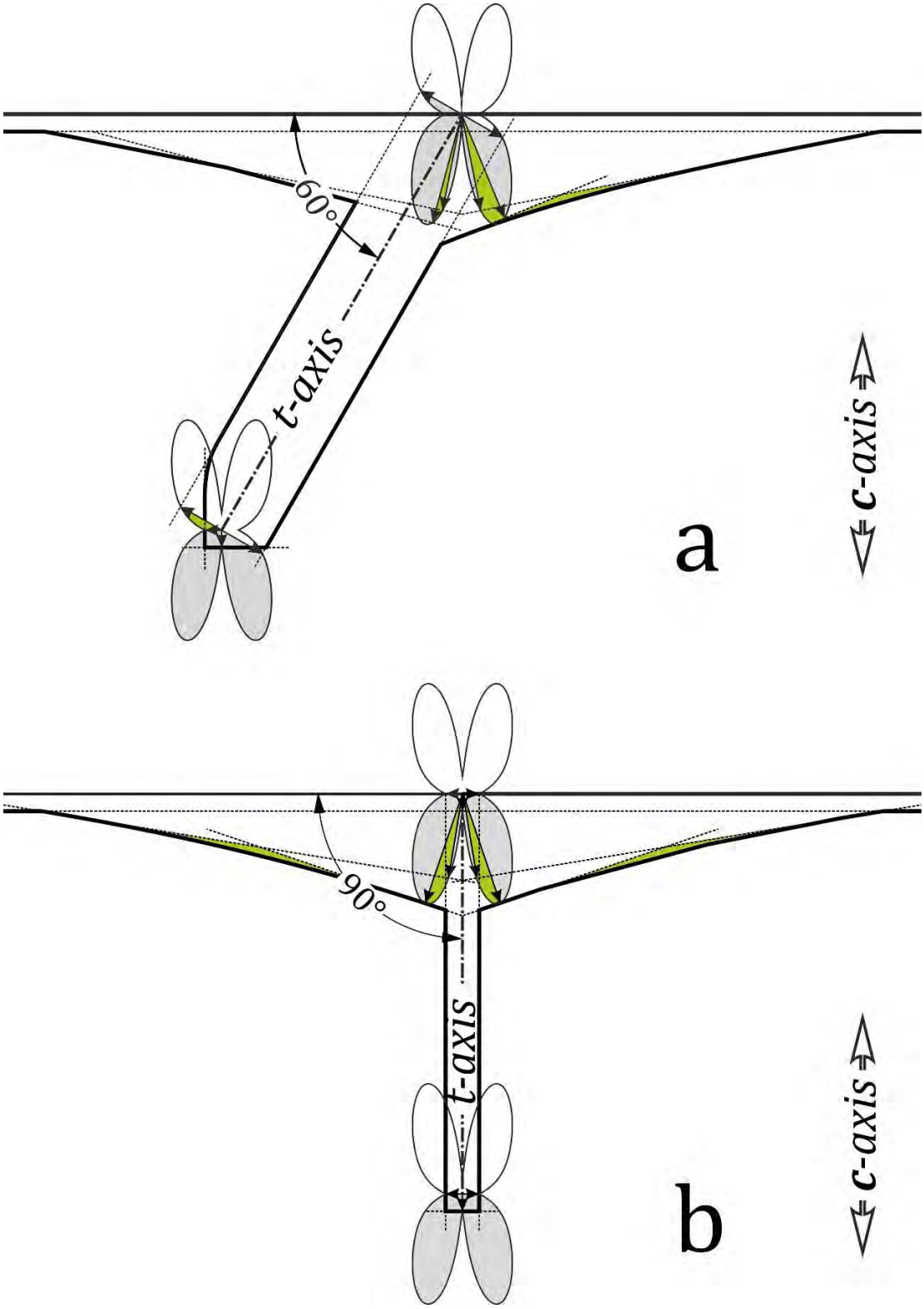

Figure 4

Always consult and cite the final, published document. See http:/www.minsocam.org or GeoscienceWorld

This is the peer-reviewed, final accepted version for American Mineralogist, published by the Mineralogical Society of America.
The published version is subject to change. Cite as Authors (Year) Title. American Mineralogist, in press.
DOI: https://doi.org/10.2138/am-2022-8055. http://www.minsocam.org/

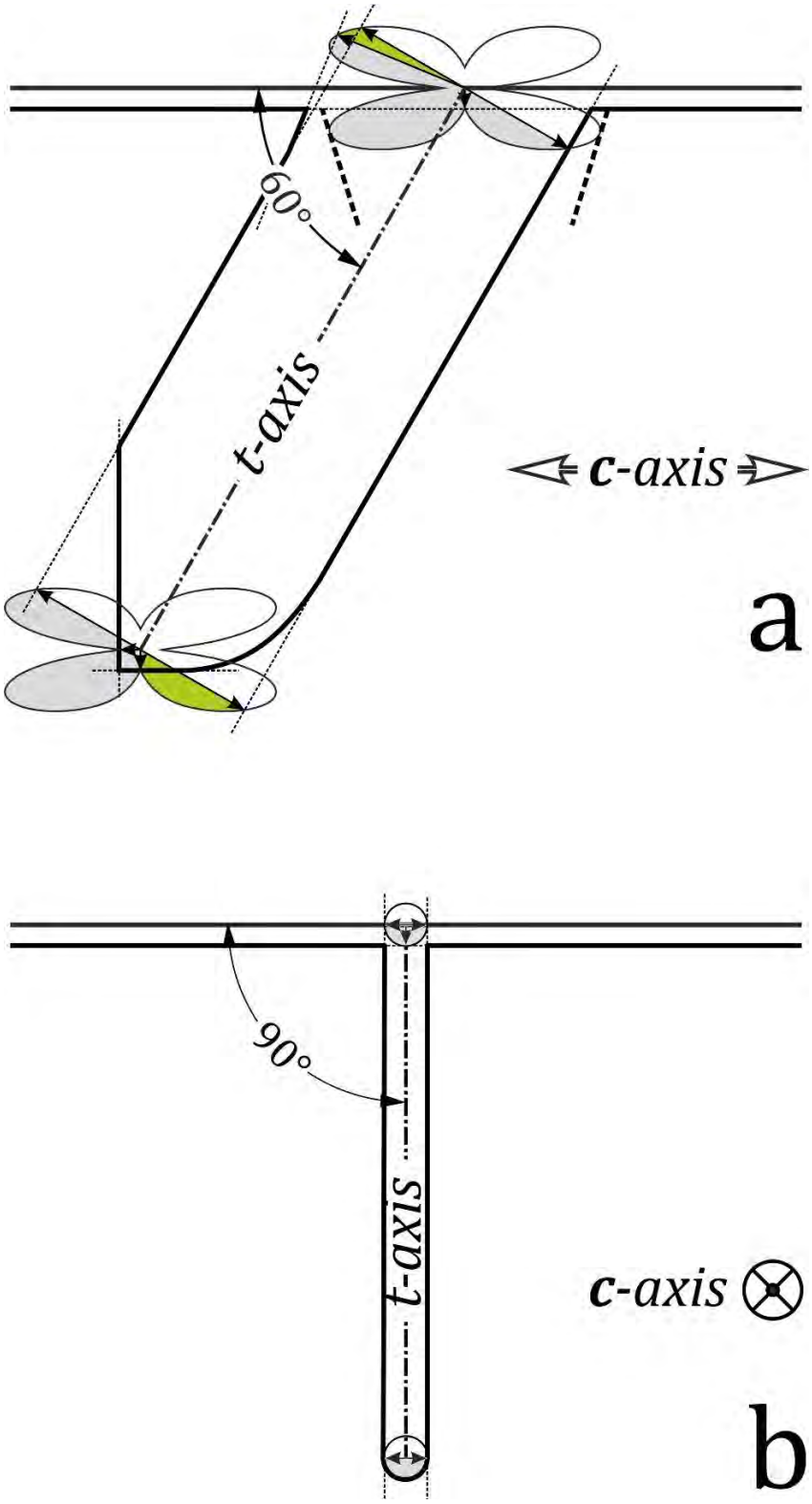

Figure 5

Always consult and cite the final, published document. See http:/www.minsocam.org or GeoscienceWorld

This is the peer-reviewed, final accepted version for American Mineralogist, published by the Mineralogical Society of America.
The published version is subject to change. Cite as Authors (Year) Title. American Mineralogist, in press.
DOI: https://doi.org/10.2138/am-2022-8055. http://www.minsocam.org/

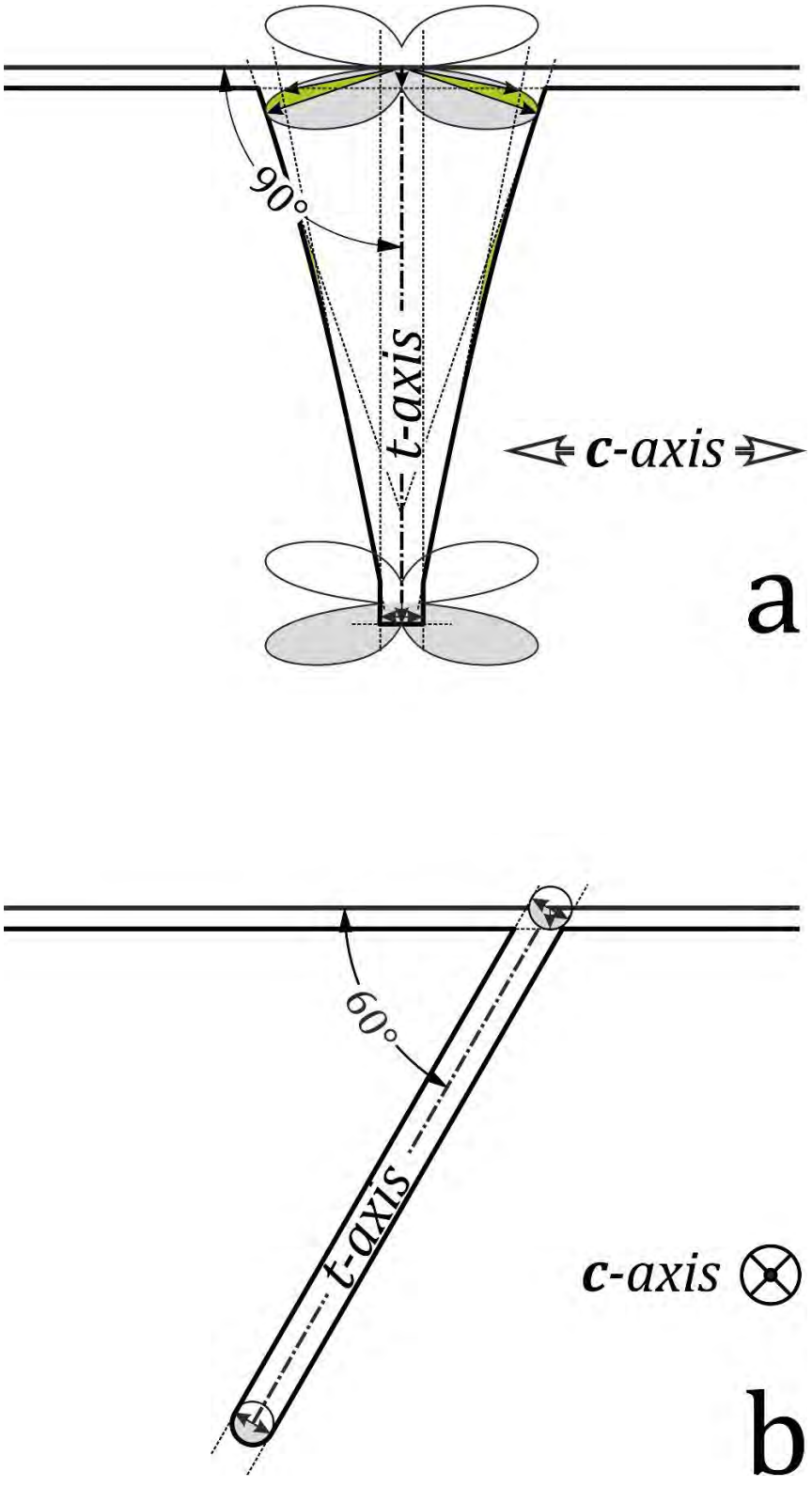

Figure 6

Always consult and cite the final, published document. See http:/www.minsocam.org or GeoscienceWorld

This is the peer-reviewed, final accepted version for American Mineralogist, published by the Mineralogical Society of America.
The published version is subject to change. Cite as Authors (Year) Title. American Mineralogist, in press.
DOI: https://doi.org/10.2138/am-2022-8055. http://www.minsocam.org/

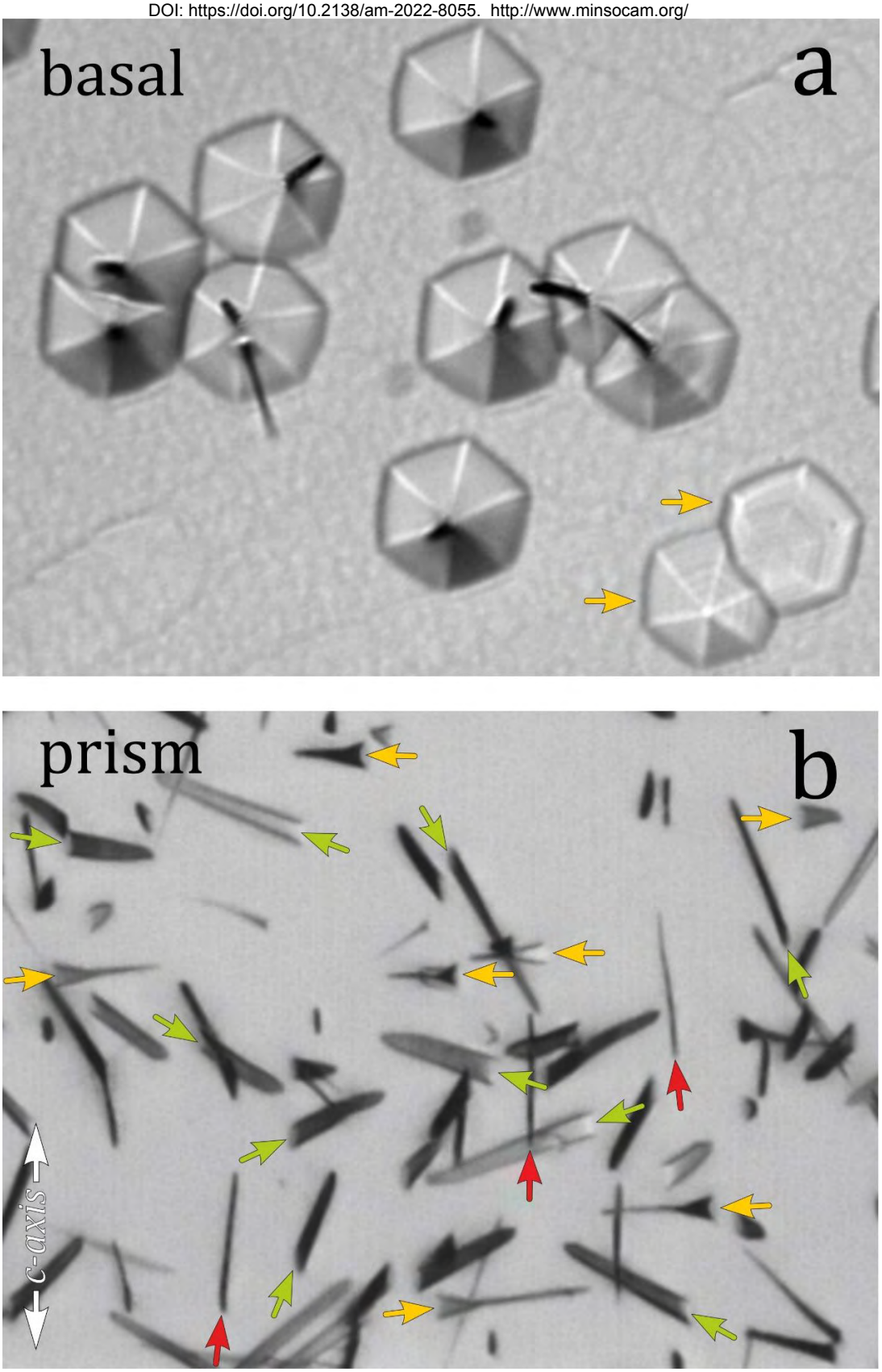

Figure 7

Always consult and cite the final, published document. See http:/www.minsocam.org or GeoscienceWorld

This is the peer-reviewed, final accepted version for American Mineralogist, published by the Mineralogical Society of America.
The published version is subject to change. Cite as Authors (Year) Title. American Mineralogist, in press.
DOI: https://doi.org/10.2138/am-2022-8055. http://www.minsocam.org/

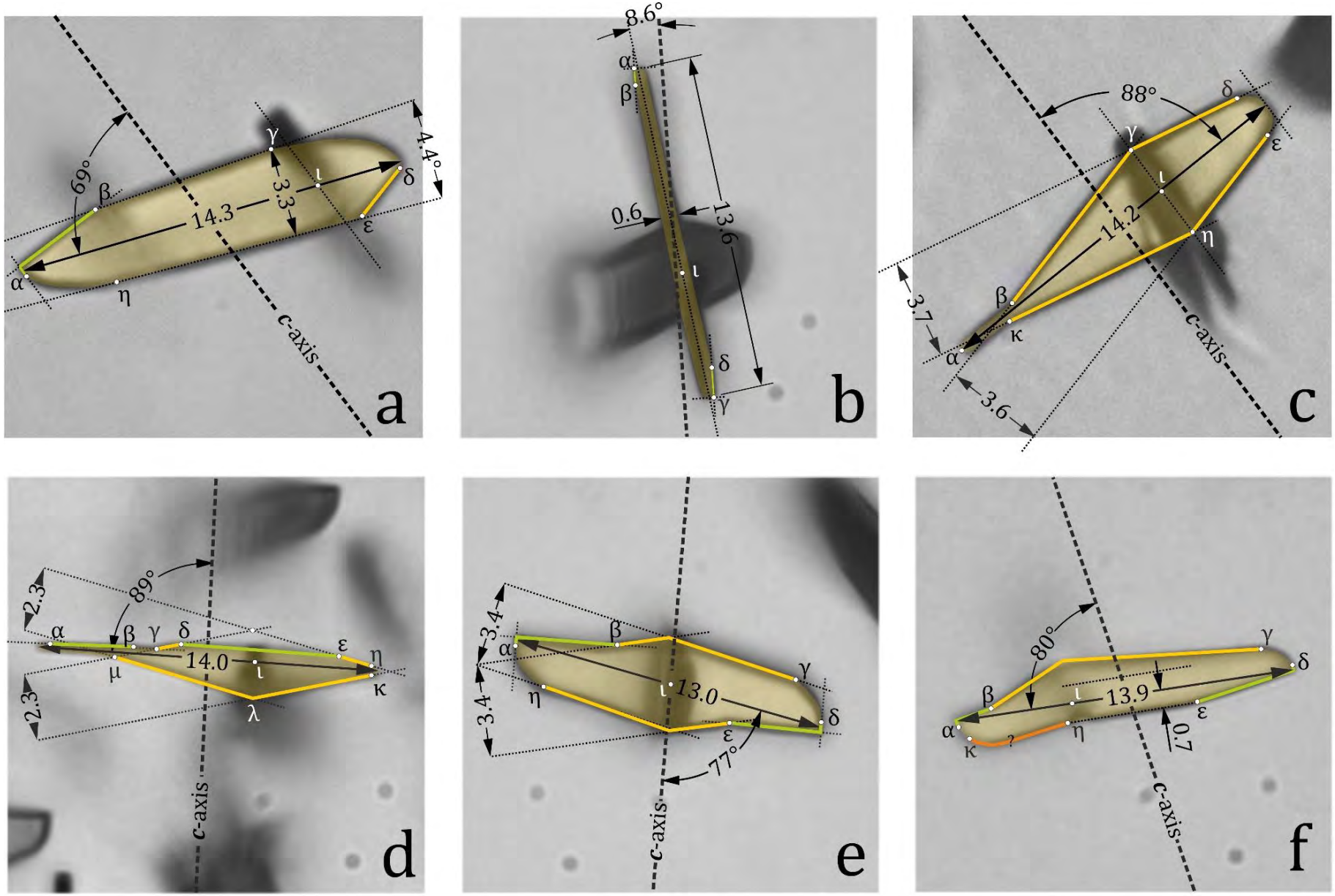

Figure 8

Always consult and cite the final, published document. See http:/www.minsocam.org or GeoscienceWorld

This is the peer-reviewed, final accepted version for American Mineralogist, published by the Mineralogical Society of America.
The published version is subject to change. Cite as Authors (Year) Title. American Mineralogist, in press.
DOI: https://doi.org/10.2138/am-2022-8055. http://www.minsocam.org/

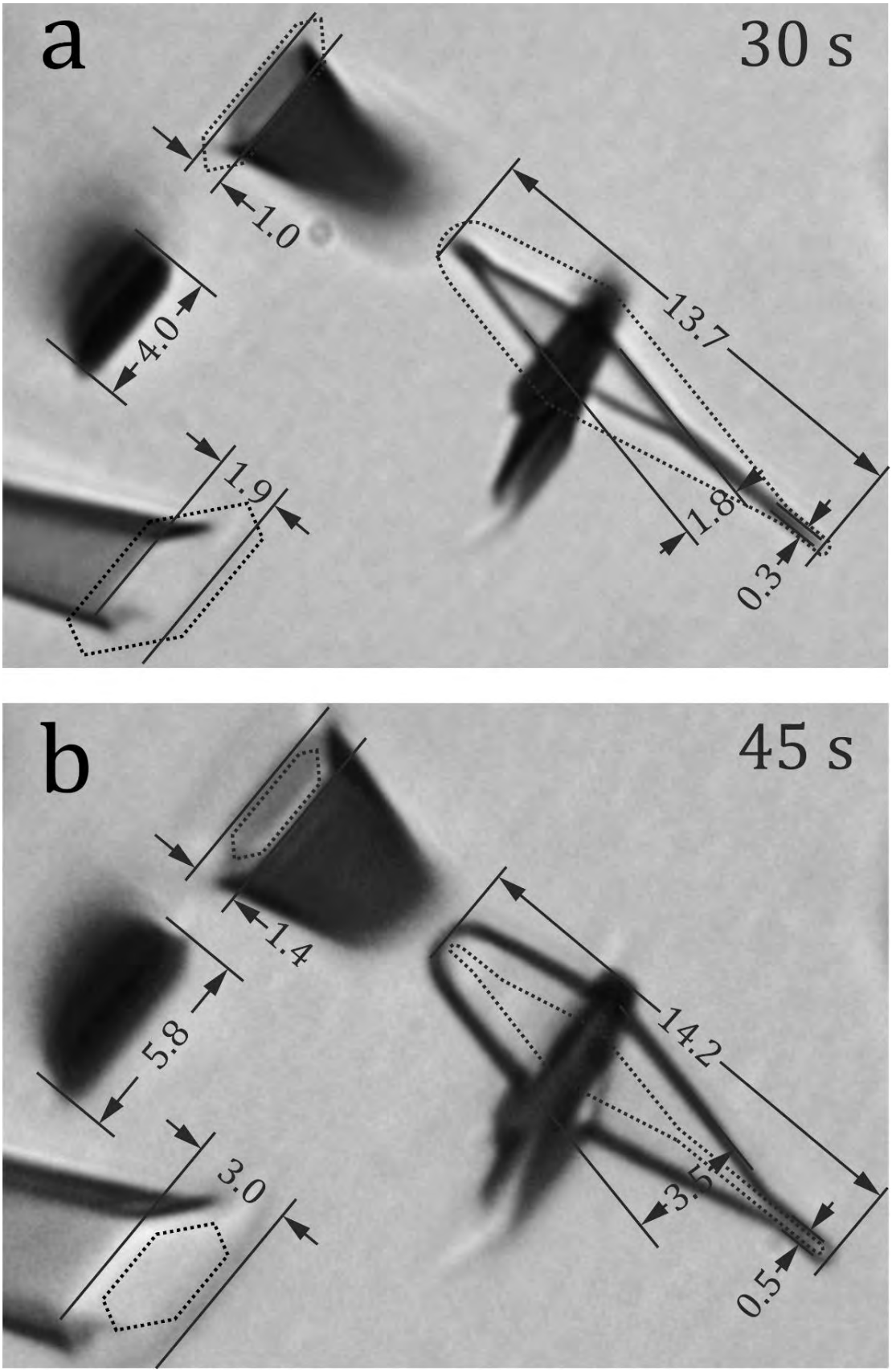

Figure 9

Always consult and cite the final, published document. See http:/www.minsocam.org or GeoscienceWorld